Supplementary Material to:

Ramūnas Digaitis, Emil E Thybring, Lisbeth G Thygesen, Maria Fredriksson, *Targeted acetylation of wood – a tool for tuning wood-water interactions*.

Table S1. The most prominent Raman peaks in native and acetylated spruce detected in the present study and their assignments according to the literature.

Wavenumber (cm^{-1})	Assignment	Reference
380	CCC, CO, CCO, aromatic ring deformation, cellulose heavy atom stretching	Wiley and Atalla (1987): 380 cm^{-1} Schenzel and Fischer (2001): 373 cm^{-1}, Adebajo et al. (2006): 378 cm^{-1}, Gierlinger et al. (2013): 380 cm^{-1}, Bock and Gierlinger (2019): 379 cm^{-1}
645	O-C=O in-plane deformation (associated with acetylation)	Adebajo et al. (2006): 654 cm^{-1}
910	HCC and HCO bending (associated with acetylation)	Wiley and Atalla (1987): 910 cm^{-1}
1095	COC glycosidic link	Adebajo et al. (2006): 1094 cm^{-1}, Gierlinger et al. (2013): 1098 cm^{-1}
1139	aromatic C-H in plane deformation	Gierlinger et al. (2013): 1139 cm^{-1}
1271	aryl-O stretching vibration of aryl-OH and aryl-O-CH_3, guaiacyl ring (with C=O group) mode	Gierlinger et al. (2013): 1271 cm^{-1}
1335	CH_2 deformation vibrations, aliphatic OH bend	Adebajo et al. (2006): 1334 cm^{-1}, Gierlinger et al. (2013): 1334 cm^{-1}
1375	CH_2 deformation vibrations	Adebajo et al. (2006): 1378 cm^{-1}
1459	C-H_3 deformation in O-CH_3, C-H_2 scissoring or guaiacyl ring vibration	Gierlinger et al. (2013): 1458 cm^{-1}
1599	symmetric aryl ring stretching	Gierlinger et al. (2013): 1599 cm^{-1}
1657	ring-conjugated C=C stretching of coniferyl alcohol	Gierlinger et al. (2013): 1657 cm^{-1}
1735	*v*(C=O) carbonyl stretching of ester (associated with acetylation)	Adebajo et al. (2006): 1735 cm^{-1}
2895	CH and CH_2 stretching	Wiley and Atalla (1987): 2889 cm^{-1}
2941	CH stretch of the methoxy group (associated with acetylation)	Bock and Gierlinger (2019): 2941 cm^{-1}
3365	OH stretching	Wiley and Atalla (1987): 3363 cm^{-1}

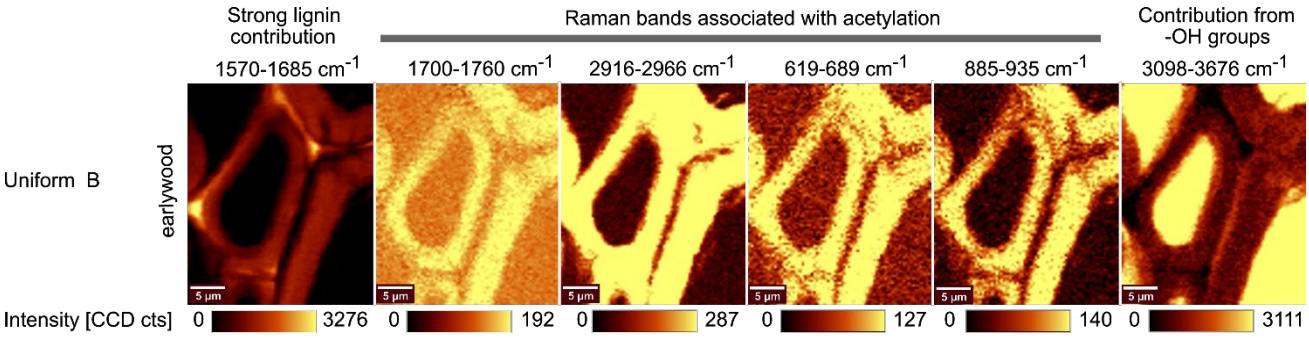

Figure S1. Raman images of a uniformly acetylated earlywood cross section (modification B) obtained by integrating over defined wavenumber areas. Column 1: intensity of the aromatic lignin band at 1570-1685 cm^{-1}, column 2: intensity of the C=O stretching at 1700-1760 cm^{-1}, column 3: intensity of C-H stretching at 2916-2966 cm^{-1}, column 4: intensity of O-C=O deformation at 619-689 cm^{-1}, column 5: intensity of HCC and HCO bending at 885-935 cm^{-1} and column 6: intensity of OH stretching at 3098-3676 cm^{-1}.

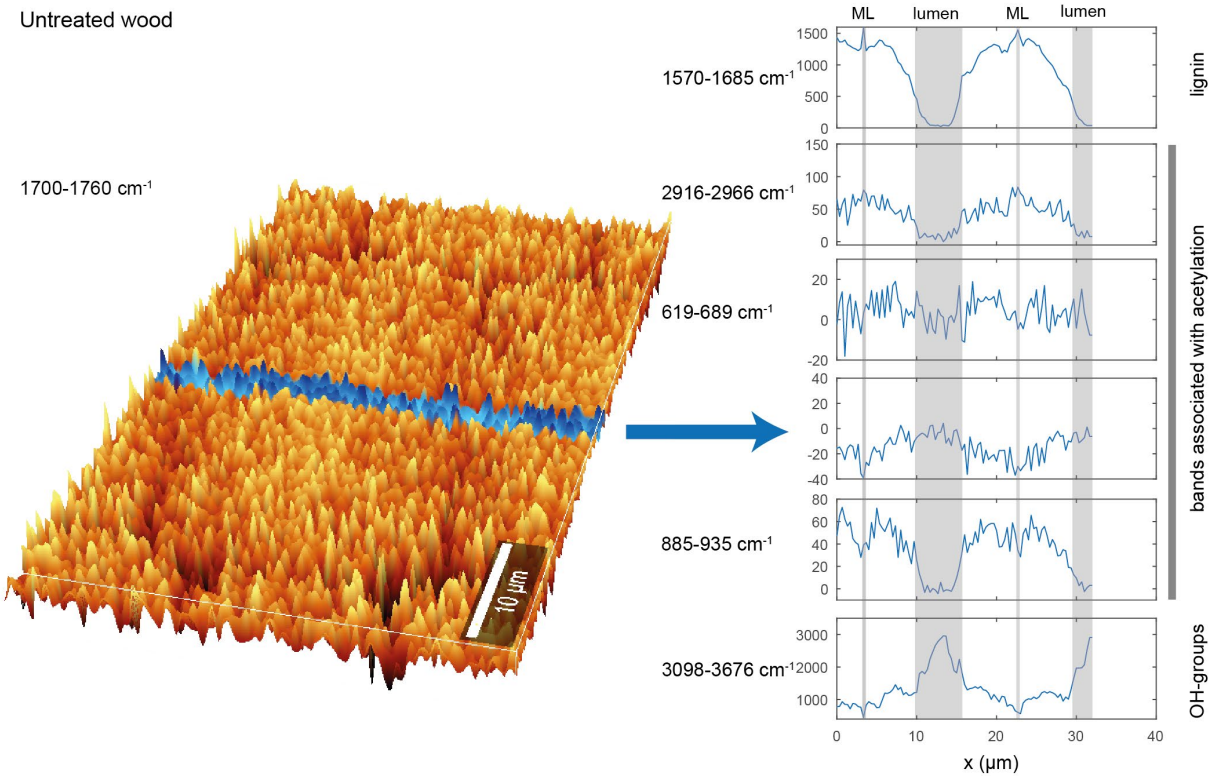

Figure S2. 3D visualisation of the 1700-1760 cm^{-1} band as well as profiles of this and the other evaluated bands through one untreated latewood cell. The approximate positions of middle lamellas (ML) and lumina along the specific cell wall section (x) were estimated visually from the Raman image of lignin signal (integration range, 1570-1685 cm^{-1}) at the centre of the 3 µm wide band shown in the 3D Raman image.

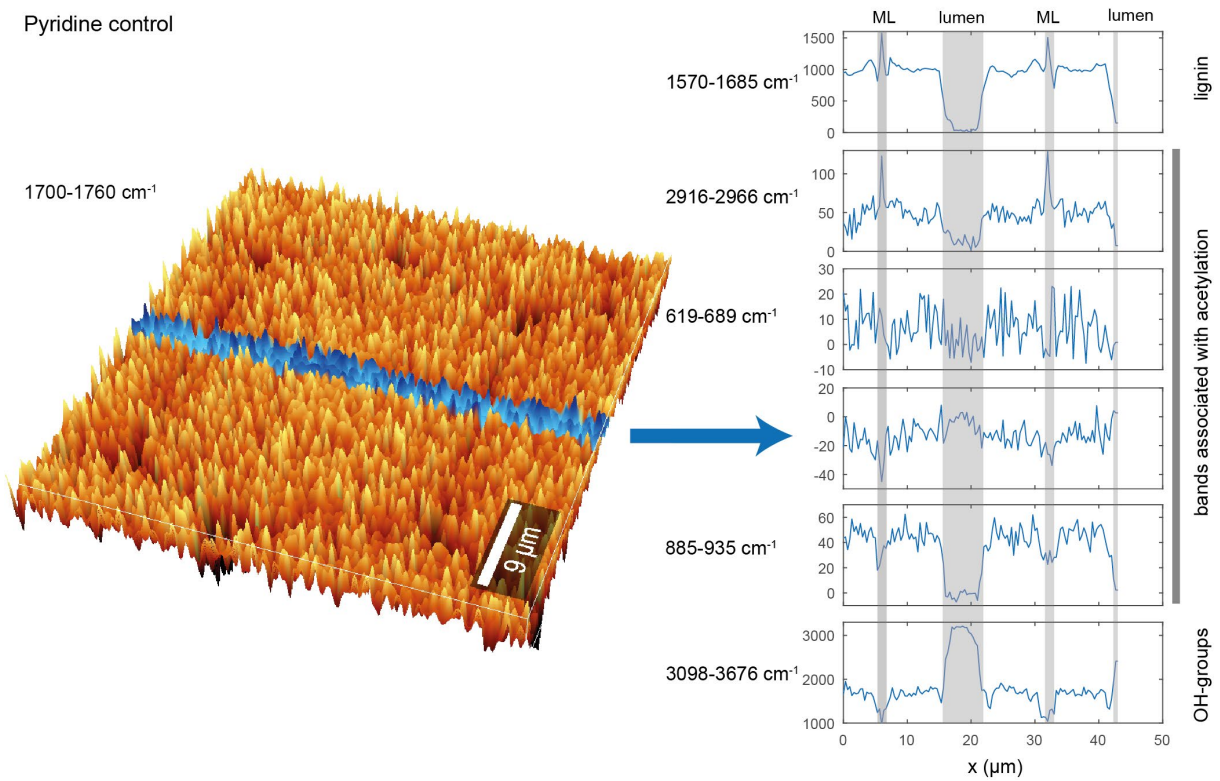

Figure S3. 3D visualisation of the 1700-1760 cm^{-1} band as well as profiles of this and the other evaluated bands through one latewood cell treated only with pyridine (references). The approximate positions of middle lamellas (ML) and lumina along the specific cell wall section (*x*) were estimated visually from the Raman image of lignin signal (integration range, 1570-1685 cm^{-1}) at the centre of the 3 µm wide band shown in the 3D Raman image.

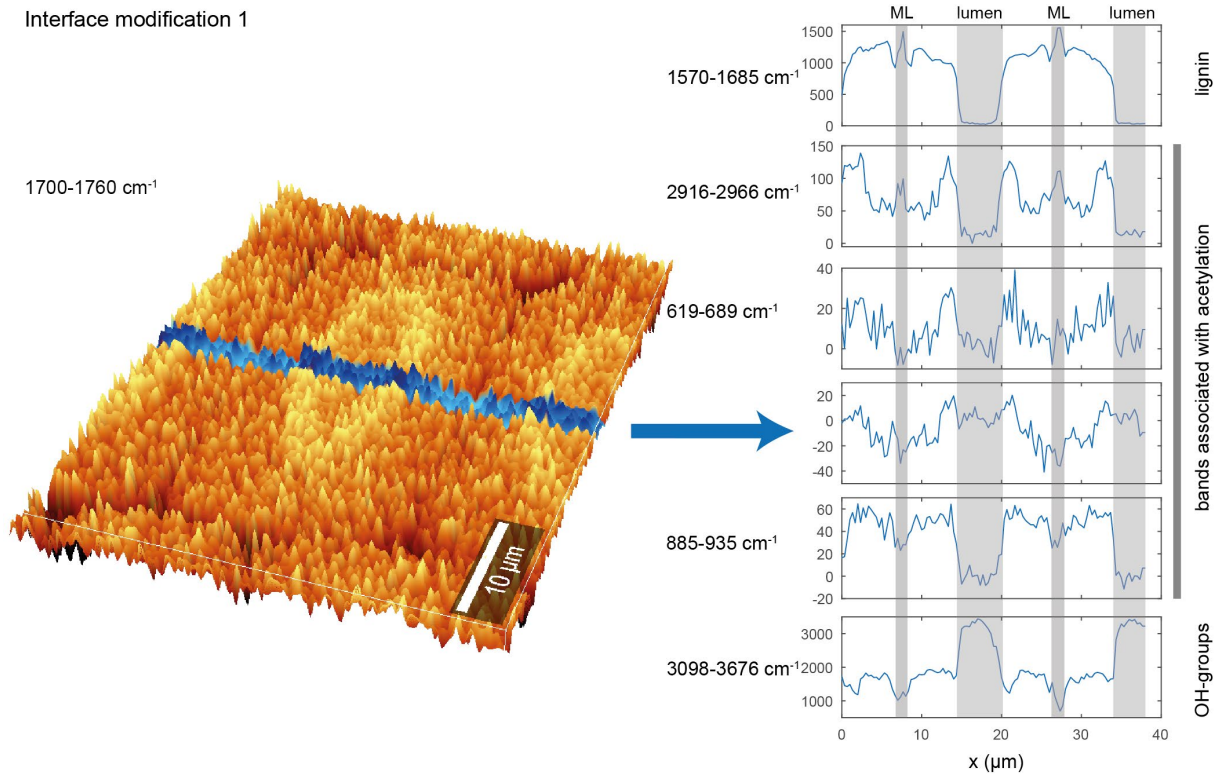

Figure S4. 3D visualisation of the 1700-1760 cm^{-1} band as well as profiles of this and the other evaluated bands through interface modified latewood cells (interface modification 1). The approximate positions of middle lamellas (ML) and lumina along the specific cell wall section (*x*) were estimated visually from the Raman image of lignin signal (integration range, 1570-1685 cm^{-1}) at the centre of the 3 µm wide band shown in the 3D Raman image.

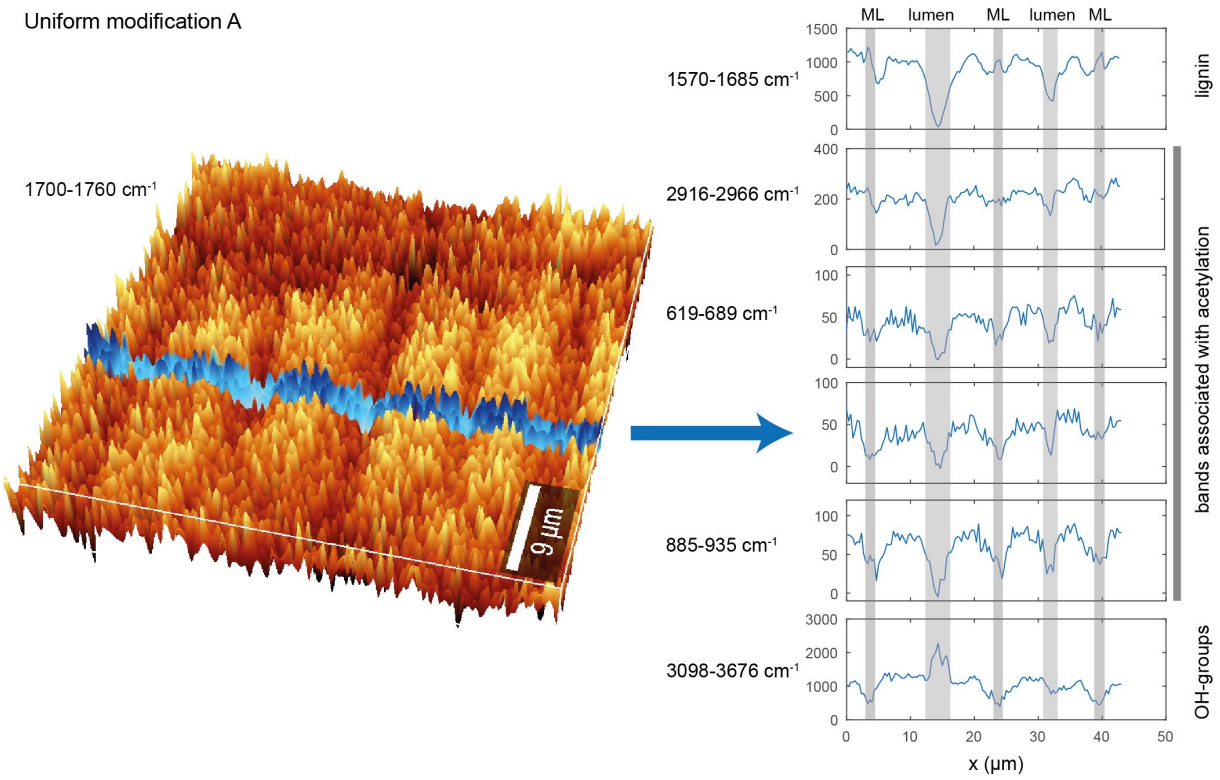

Figure S5. 3D visualisation of the 1700-1760 cm^{-1} band as well as profiles of this and the other evaluated bands through two uniformly modified latewood cells (uniform modification A). The approximate positions of middle lamellas (ML) and lumina along the specific cell wall section (*x*) were estimated visually from the Raman image of lignin signal (integration range, 1570-1685 cm^{-1}) at the centre of the 3 µm wide band shown in the 3D Raman image.

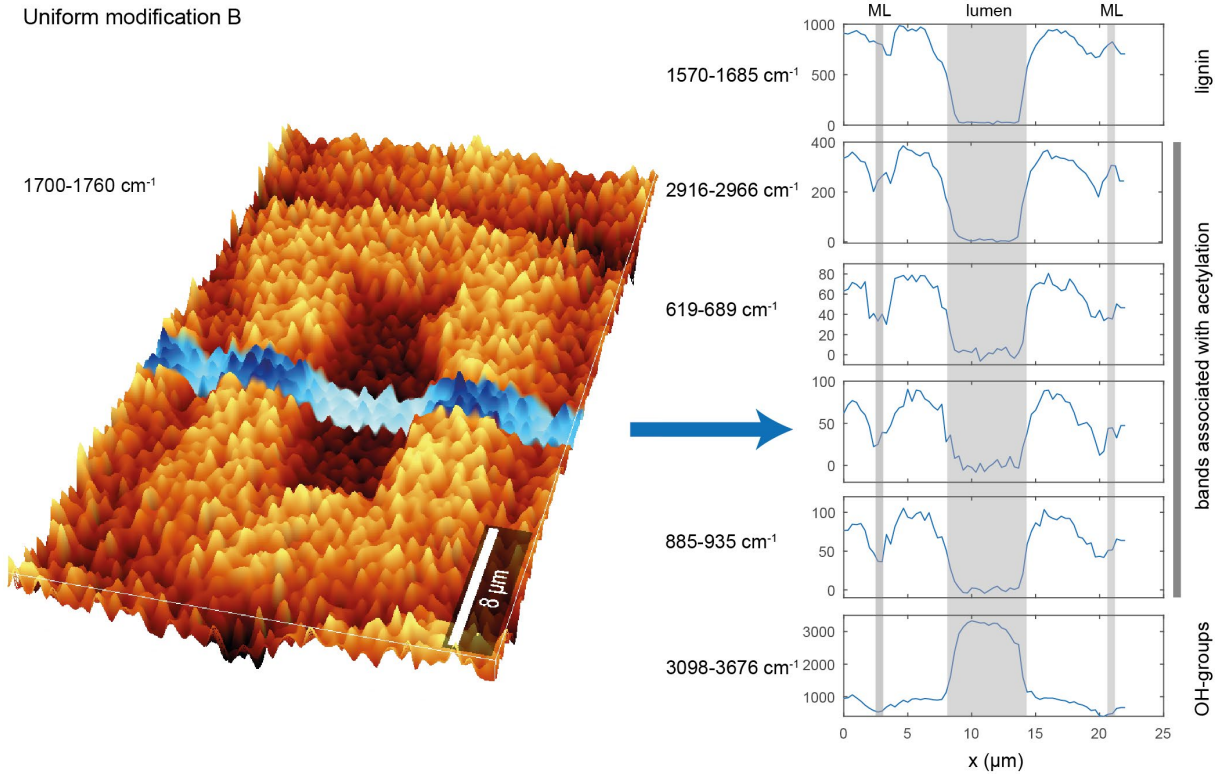

Figure S6. 3D visualisation of the 1700-1760 cm^{-1} band as well as profiles of this and the other evaluated bands through one uniformly modified latewood cell (uniform modification B). The approximate positions of middle lamellas (ML) and lumina along the specific cell wall section (*x*) were estimated visually from the Raman image of lignin signal (integration range, 1570-1685 cm^{-1}) at the centre of the 3 µm wide band shown in the 3D Raman image.

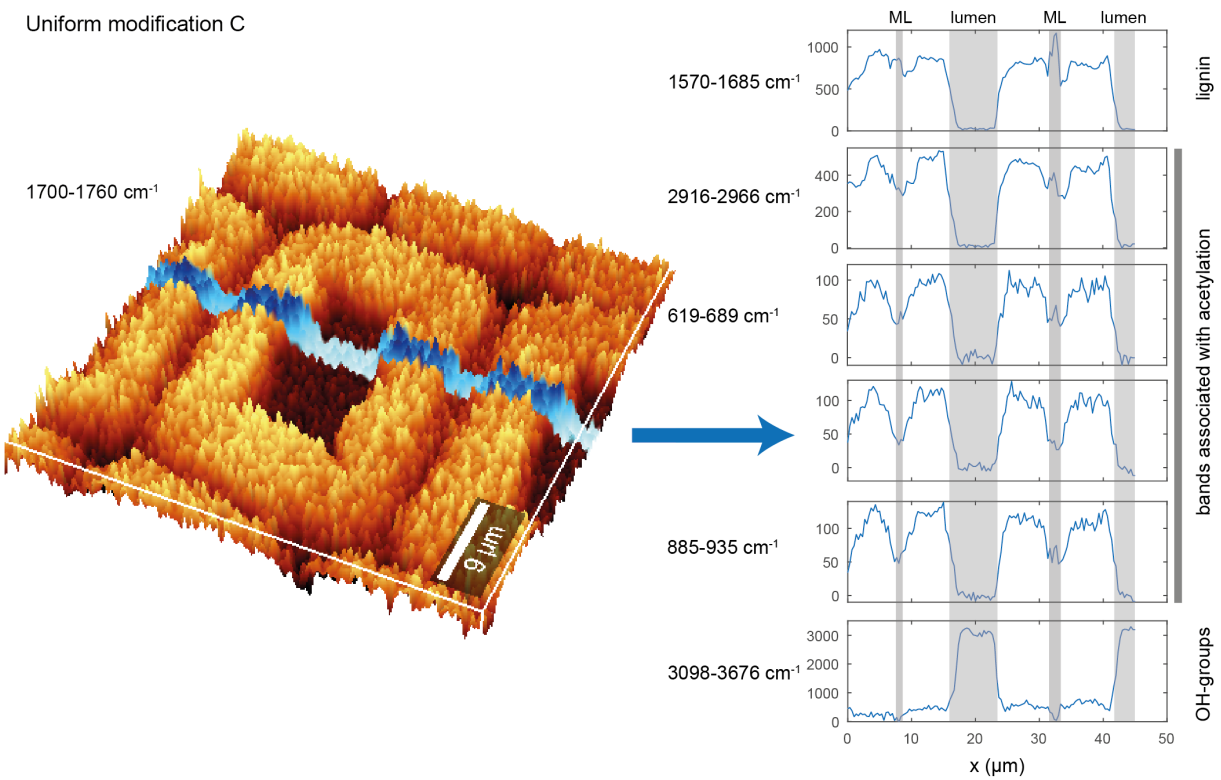

Figure S7. 3D visualisation of the 1700-1760 cm^{-1} band as well as profiles of this and the other evaluated bands through uniformly modified latewood cells (uniform modification C). The approximate positions of middle lamellas (ML) and lumina along the specific cell wall section (*x*) were estimated visually from the Raman image of lignin signal (integration range, 1570-1685 cm^{-1}) at the centre of the 3 µm wide band shown in the 3D Raman image.

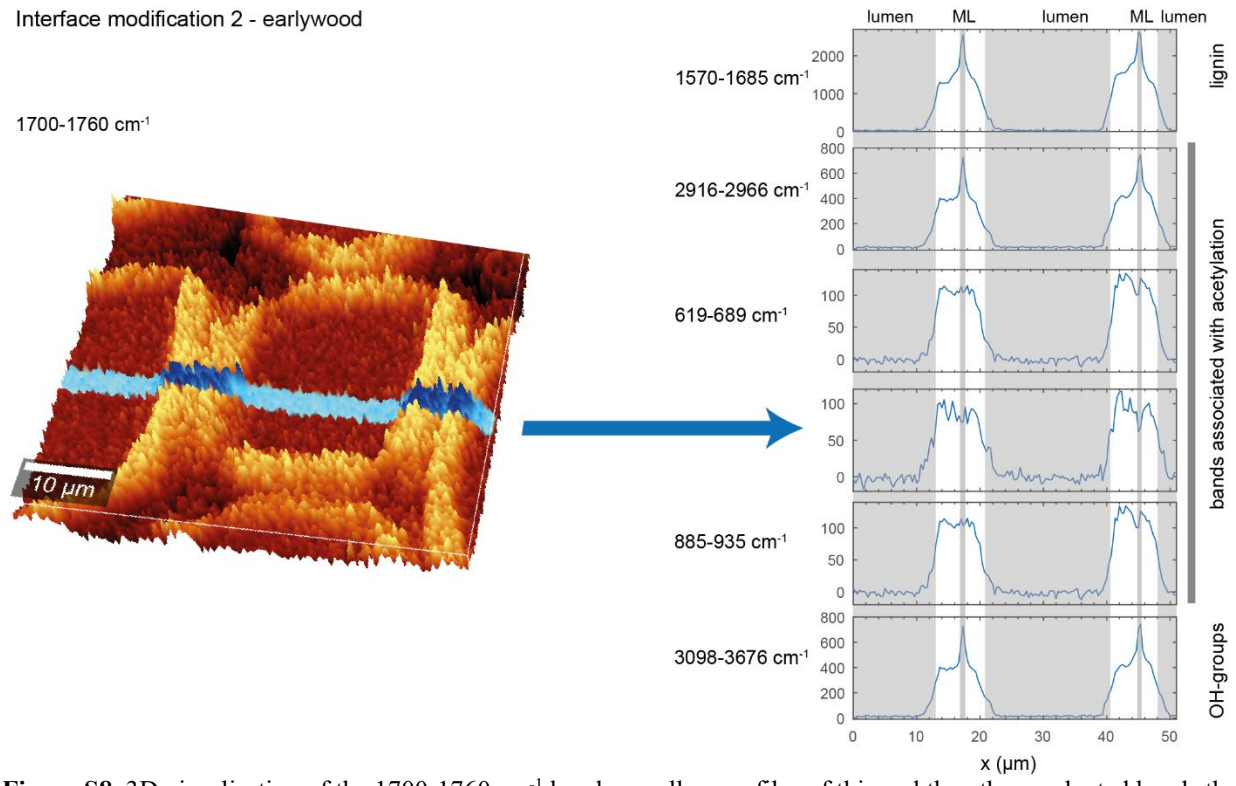

Figure S8. 3D visualisation of the 1700-1760 cm^{-1} band as well as profiles of this and the other evaluated bands through interface modified earlywood cells (interface modification 2). The approximate positions of middle lamellas (ML) and lumina along the specific cell wall section (*x*) were estimated visually from the Raman image of lignin signal (integration range, 1570-1685 cm^{-1}) at the centre of the 3 µm wide band shown in the 3D Raman image.

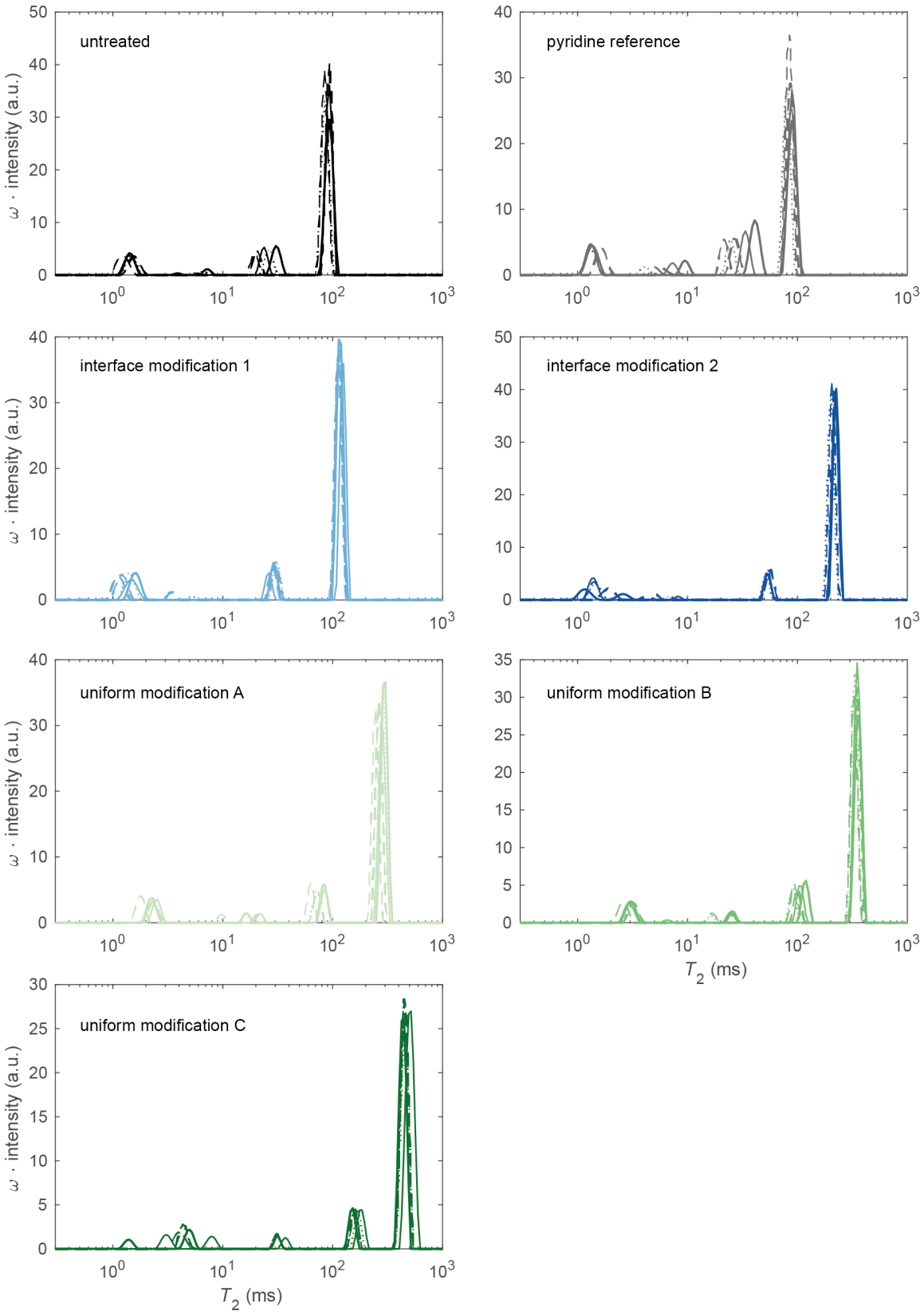

Figure S9. LFNMR data for individual specimens. Average data are shown in Figure 5 in the main manuscript.

Table S2. Individual mass change after modifications (R_{mod}) for the interface modified specimens used in the LFNMR measurements.

modification	replicate	R_{mod} (g g^{-1})
Interface 1	1	0.0433
	2	0.0305
	3	0.0429
	4	0.0424
	5	0.0356
Interface 2	1	0.0956
	2	0.0924
	3	0.0999
	4	0.1031
	5	0.1136

Table S3. Total moisture content, moisture content corresponding to capillary water and cell wall moisture contents for water saturated specimens used in the LFNMR experiments. The total moisture content was determined gravimetrically, while the capillary water moisture content and the cell wall moisture content was evaluated from the LFNMR-data. The average values from these data are shown in Figure 6 in the main manuscript. This table also includes moisture exclusion efficiency, which was evaluated from the cell wall moisture content. Average data and standard deviations are shown in Figure 7b. Note that the cell wall moisture content is underestimated using this method (Beck et al. 2018; Telkki et al. 2013; Thybring et al. 2020) so the absolute values of the cell wall moisture content should be interpreted with care. All data in this table has been corrected for mass change caused by the modification.

			interface modification		uniform modification		
replicate	untreated	pyridine controls	1	2	A	B	C
total moisture content (g g^{-1})							
1	2.220	2.222	2.295	2.173	2.136	1.978	1.790
2	2.155	2.320	1.994	2.011	2.019	2.028	1.994
3	2.295	2.187	2.088	2.190	1.963	1.885	1.866
4	2.181	2.258	2.179	2.132	1.830	1.918	1.896
5	2.241	2.048	2.152	2.042	2.046	1.853	1.825
capillary moisture content (g g^{-1})							
1	1.966	1.917	2.014	2.009	1.925	1.789	1.602
2	1.897	2.008	1.737	1.773	1.810	1.867	1.810
3	2.039	1.895	1.842	2.025	1.755	1.708	1.718
4	1.909	1.954	1.921	1.930	1.604	1.747	1.745
5	2.003	1.775	1.882	1.838	1.829	1.678	1.676
cell wall moisture contents (g g^{-1})							
1	0.254	0.30	0.281	0.164	0.211	0.189	0.188
2	0.259	0.312	0.257	0.239	0.208	0.161	0.184
3	0.256	0.292	0.246	0.165	0.208	0.177	0.148
4	0.272	0.303	0.258	0.202	0.226	0.171	0.151
5	0.238	0.273	0.270	0.204	0.217	0.175	0.149
moisture exclusion efficiency (-)							
1	0.00	-0.20	-0.11	0.36	0.17	0.26	0.26
2	0.00	-0.21	0.01	0.08	0.19	0.38	0.29
3	0.00	-0.14	0.04	0.35	0.19	0.31	0.42
4	0.00	-0.11	0.05	0.26	0.17	0.37	0.45
5	0.00	-0.15	-0.13	0.14	0.09	0.27	0.37

Table S4. Moisture content data and moisture exclusion efficiency data obtained at the different relative humidity (RH) levels in the hygroscopic range using a sorption balance in both desorption and absorption. These data were the basis for evaluation of the moisture exclusion efficiency shown in Figure 7b in the main manuscript. All data in this table have been corrected for mass change caused by the modification according to the R_{mod} values given in this table.

			interface modification		uniform modification		
RH	**untreated**	**pyridine refs.**	**1**	**2**	**A**	**B**	**C**
R:	**0**	**0**	**0.0324**	**0.098**	**0.1283**	**0.1419**	**0.2087**
moisture contents (g g^{-1})							
95%	0.299	0.300	0.276	0.253	0.257	0.193	0.179
80%	0.204	0.204	0.187	0.170	0.170	0.137	0.130
65%	0.157	0.158	0.142	0.127	0.125	0.101	0.095
50%	0.122	0.121	0.109	0.095	0.092	0.072	0.066
35%	0.092	0.092	0.081	0.069	0.066	0.051	0.046
0	0.000	0.000	0.000	0.000	0.000	0.000	0.001
35%	0.076	0.075	0.068	0.058	0.054	0.042	0.038
50%	0.099	0.097	0.089	0.077	0.074	0.057	0.052
65%	0.128	0.126	0.116	0.101	0.098	0.077	0.072
80%	0.170	0.167	0.157	0.137	0.134	0.105	0.097
95%	0.252	0.244	0.237	0.202	0.201	0.148	0.135
moisture exclusion efficiency (g g^{-1})							
95%	0	0.00	0.07	0.15	0.14	0.35	0.40
80%	0	0.00	0.08	0.17	0.17	0.33	0.36
65%	0	-0.01	0.09	0.19	0.20	0.36	0.40
50%	0	0.01	0.11	0.22	0.24	0.41	0.46
35%	0	0.01	0.12	0.25	0.29	0.45	0.50
0							
35%	0	0.01	0.11	0.24	0.28	0.44	0.50
50%	0	0.02	0.10	0.22	0.25	0.42	0.47
65%	0	0.01	0.09	0.21	0.23	0.39	0.44
80%	0	0.02	0.08	0.19	0.21	0.38	0.43
95%	0	0.03	0.06	0.20	0.20	0.41	0.46

References

Adebajo MO, Frost RL, Kloprogge JT, Kokot S (2006) Raman spectroscopic investigation of acetylation of raw cotton. Spectrochim Acta, Part A 64:448-453 https://doi.org/https://doi.org/10.1016/j.saa.2005.07.045

Beck G, Thybring Emil E, Thygesen Lisbeth G, Hill C (2018) Characterization of moisture in acetylated and propionylated radiata pine using low-field nuclear magnetic resonance (LFNMR) relaxometry. Holzforschung 72:225-233 https://doi.org/10.1515/hf-2017-0072

Bock P, Gierlinger N (2019) Infrared and Raman spectra of lignin substructures: Coniferyl alcohol, abietin, and coniferyl aldehyde. J Raman Spectrosc 50:778-792 https://doi.org/https://doi.org/10.1002/jrs.5588

Gierlinger N, Keplinger T, Harrington M, Schwanninger M (2013) Raman imaging of lignocellulosic feedstock. In: van de Ven T, Kadla J (eds) Cellulose - Biomass Conversion. IntechOpen Limited, London, UK, pp 159-192

Schenzel K, Fischer S (2001) NIR FT Raman Spectroscopy–a Rapid Analytical Tool for Detecting the Transformation of Cellulose Polymorphs. Cellulose 8:49-57 https://doi.org/10.1023/A:1016616920539

Telkki VV, Yliniemi M, Jokisaari J (2013) Moisture in softwoods: fiber saturation point, hydroxyl site content, and the amount of micropores as determined from NMR relaxation time distributions. Holzforschung 67:291-300 https://doi.org/10.1515/hf-2012-0057

Thybring EE, Digaitis R, Nord-Larsen T, Beck G, Fredriksson M (2020) How much water can wood cell walls hold? A triangulation approach to determine the maximum cell wall moisture content. PLoS ONE 15:e0238319 https://doi.org/10.1371/journal.pone.0238319

Wiley JH, Atalla RH (1987) Band assignments in the raman spectra of celluloses. Carbohydr Res 160:113-129 https://doi.org/https://doi.org/10.1016/0008-6215(87)80306-3